Colorimetric detector of oxidizing metal ions by anilide-poly(phenylacetylene)s

Manuel Núñez-Martínez,‡ Manuel Fernández-Míguez,‡, Emilio Quiñoá and Félix Freire*

Center for Research in Biological Chemistry and Molecular Materials (CIQUS) and Department of Organic Chemistry, University of Santiago de Compostela, E-15782 Santiago de Compostela, Spain

‡ *These authors contributed equally to this work.*

Email: felix.freire@usc.es

http://felixfreire.com

Electronic Supporting Information

Table of Contents

1. Materials and methods

Commercially available chemicals have been used as delivered. Solvents were purchased as reagent grade and distilled if necessary. Anhydrous solvents were either purchased as ultra-dry solvent from Acros Organics® or received from solvent purification system. For the coupling and polymerization reactions, dry THF was obtained from MBRAUN SPS 800 solvent purification system. Water was purified by Millipore water purification system. $Fe(ClO_4)_n$ (98.000% purity), $FeCl_3$ (99.990% purity), $AuCl_3$ (99.9%), $Cu(ClO_4)_2$ (98% purity), $Hg(ClO_4)_2$ (99.998% purity), $(NH_4)_2[Ce(NO_3)_6]$ (98.5% purity) salts were purchased from Sigma Aldrich.

NMR experiments were carried out in a Varian Inova 2 (250 MHz resonance 1H). Size exclusion chromatography studies were performed on Alliance 2695 HPLC System (Waters) liquid chromatography system equipped with a UV 2489 detector (Waters). The samples were eluted by three Phenogel columns connected to each other with stacionary phases of 10^3, 10^4 and 10^5 Amstrong and packed with a solid support of a cross-linked stiyrene and *p*-divinylbenzene copolymer.

CD measurements were done in a Jasco-720 spectropolarimeter. UV spectra were registered in a Jasco-730 spectrophotometer.

FT-IR measurements were carried out on a Bruker IFS-66v while Raman measurements were carried out in a Renishaw confocal Raman spectrophotometer (Invia Reflex model), equipped with two lasers (diode laser 785 nm and Ar laser 514 nm).

EPR experiments were carried out in a Bruker EMX with a frequency around 9.443 GHz and using perylene in H_2SO_4 as internal reference. XPS analysis of the samples was performed using a Thermo Scientific K-Alpha ESCA instrument equipped with aluminium Kα monochromatized radiation at 1486.6 eV X-ray source. Due the no conductor nature of samples was necessary to use an electron flood gun to minimize surface charging. Neutralization of the surface charge was performed by using both a low energy flood gun (electrons in the range 0 to 14 eV) and a low energy Argon ions gun.

The XPS measurements were carried out using monochromatic Al-Kα radiation (hn = 1486.6 eV). Photoelectrons were collected from a take-off angle of 90º relative to the sample surface. The measurement was done in a Constant Analyser Energy mode (CAE) with a 100 eV pass energy for survey spectra and 20eV pass energy for high resolution spectra. Charge referencing was done by setting the lower binding energy C 1s photo peak at 284.8.0 eV C1s

hydrocarbon peak. Surface elemental composition was determined using the standard Scofield photoemission cross sections.

2. Monomers and polymers

The preparation of monomers (M-**1**, M-**2**, M-**3**, M-**4**, M-**5**, M-**6**, and M-**7**) polymers (poly-**1**, poly-**2**, poly-**3**, poly-**4**, poly-**5**, poly-**6**, and poly-**7**) can be found in references [S1], [S2] and [S3].

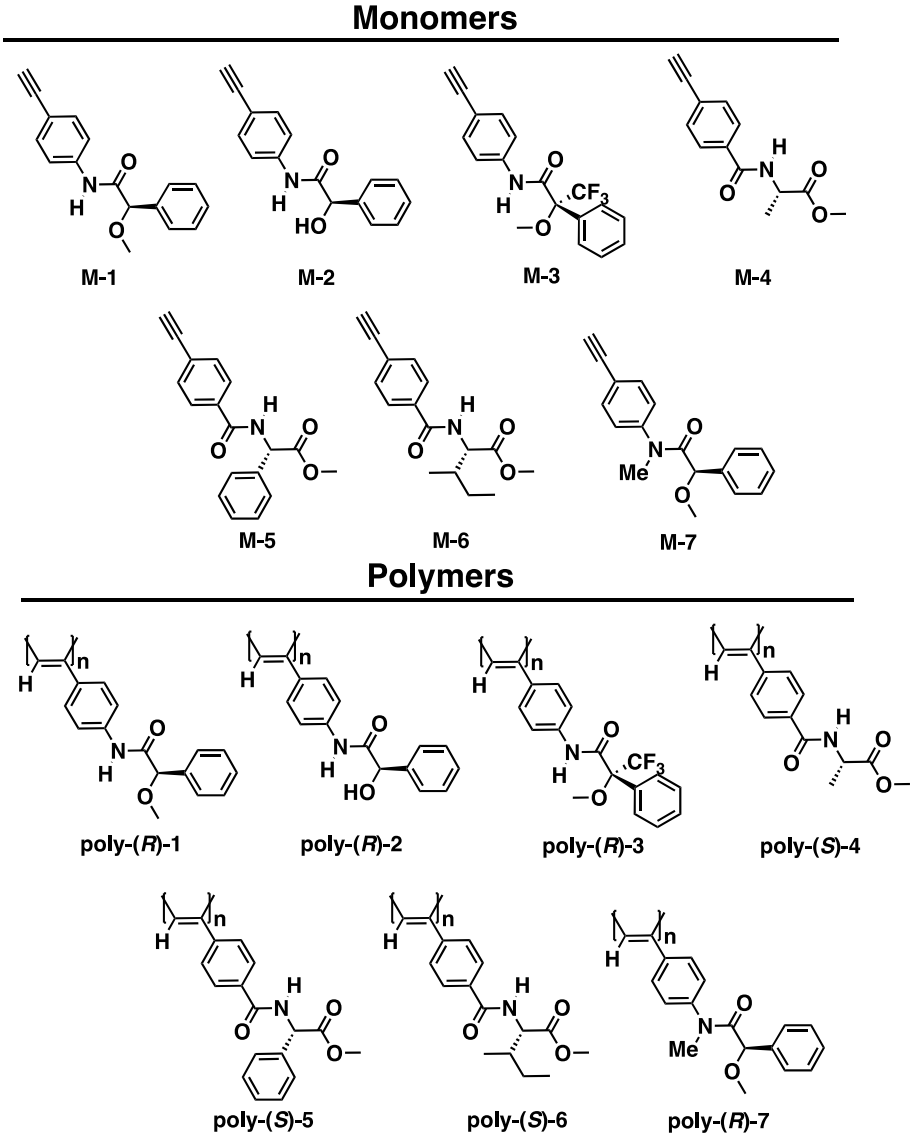

Figure S1. Structures of PPAs with anilide and bezamide connection.

3. Synthesis of monomer M-7

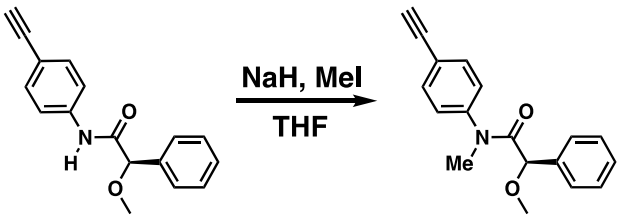

M-1 **M-7**

Sodium hydride (0.016 g, 0.416 mmol) was dissolved in dry THF (4 mL, 0° C) and M-**1** (0.100 g, 0.376 mmol) dissolved in 10 mL in dry THF was added drop by drop. After 30 min, iodomethane (0.069 g, 0.489 mmol) was added and the reaction mixture was stirred overnight at room temperature. Once the reaction was completed (checked by TLC), all the mixture was poured into ethyl acetate and washed with water three times. Afterward the organic layer was separated, dried (Na_2SO_4) and concentrated. The crude product was purified by column chromatography over silica gel using hexane/ethyl acetate (7:3 as an eluent). The solvent was removed in vacuum to obtain compound M-**7** as colorless oil (Yield 0.082 g, 79%).

Spectroscopic data:

^{1}H NMR (250 MHz, $CDCl_3$) δ (ppm): 3.14 (1H, s), 3.21 (3H, s), 4.63 (1H, s), 6.93 (2H, d), 7.10 (2H, s), 7.24 (3H, s), 7.44 (2H, d).

^{13}C NMR (62.5 MHz, $CDCl_3$) δ (ppm): 29.6, 37.8, 56.8, 80.8, 82.8, 122.1, 128.1, 128.4, 128.6, 133.3, 136.1, 143.0, 169.7.

HRMS (ESI) m/z calculated for $C_{18}H_{17}NO_2$ $[M+H]^+$: 280.1259, found: 280.1332.

$[\alpha]_D^{20}$ = +76 (13 mg mL^{-1}, $CHCl_3$)

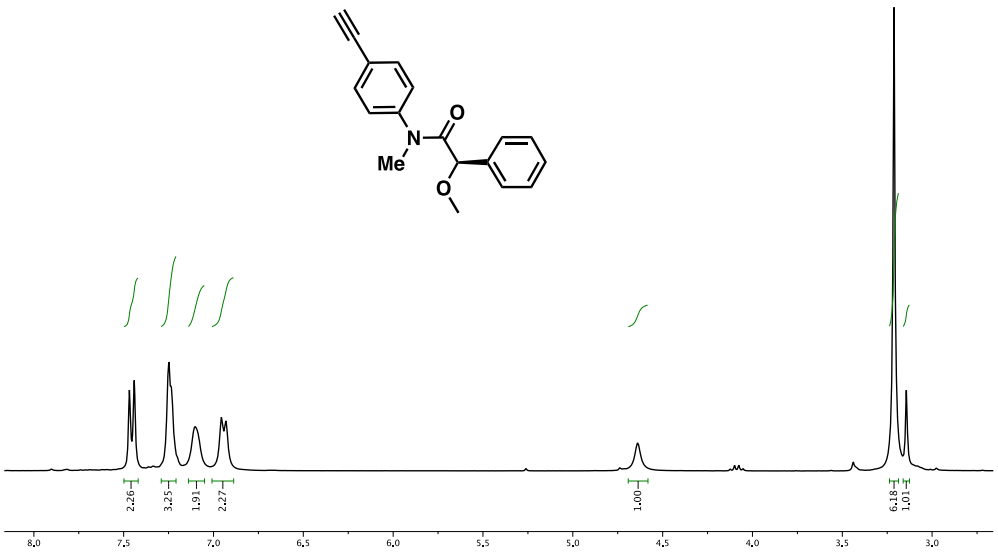

Figure S2. ^{1}H NMR of monomer M-**7.**

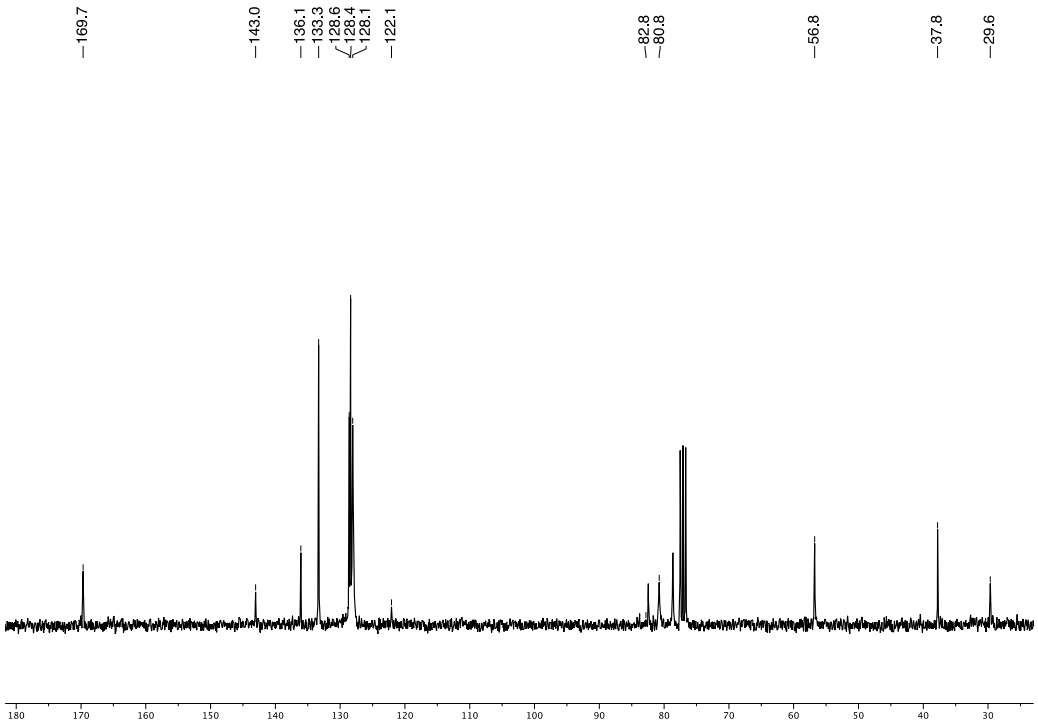

Figure S3. ^{13}C NMR of monomer M-**7.**

4. Synthesis of poly-(*R*)-7

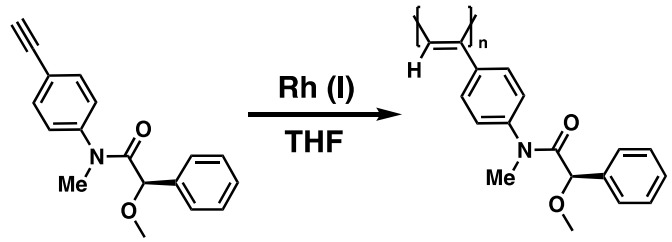

M-7 **poly-(*R*)-7**

The reaction flask (sealed ample) was dried under vacuum and Ar flushed for three times before the corresponding monomer M-**1** (100 mg) was added as a solid. Then, the flask was dried with a vacuum line and flushed with Ar (three times). Dry THF (0.72 mL) was added with a syringe and Et_3N dropwise. A solution of catalyst, $[Rh(nbd)Cl]_2$ (1.65 mg) was added at 30° C. The reaction mixture was stirred at 30°C for 24 h. The resulting polymer was diluted in CH_2Cl_2 and precipitated in a large amount of MeOH, centrifugated twice and reprecipitated using hexane and centrifugated again (92% of yield).

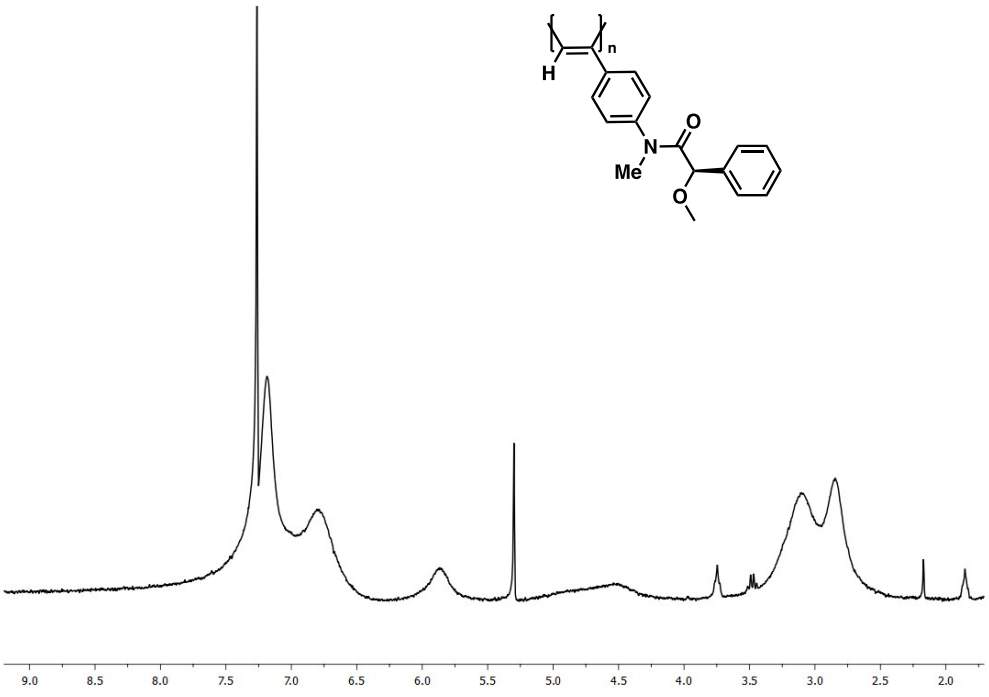

Figure S4. ^1H NMR of poly-(*R*)-**7**

5. UV-Vis studies of anilide-PPAs connection in different high polar and low polar solvents in presence of $Fe(ClO_4)_3$

UV-Vis were performed for poly-(*R*)-**1** (0.1 mg mL^{-1}) in different high polar (DMF and DMSO) and low polar solvents (THF and $CHCl_3$) using $Fe(ClO_4)_3$ which concentration was 10.0 mg mL^{-1} THF.

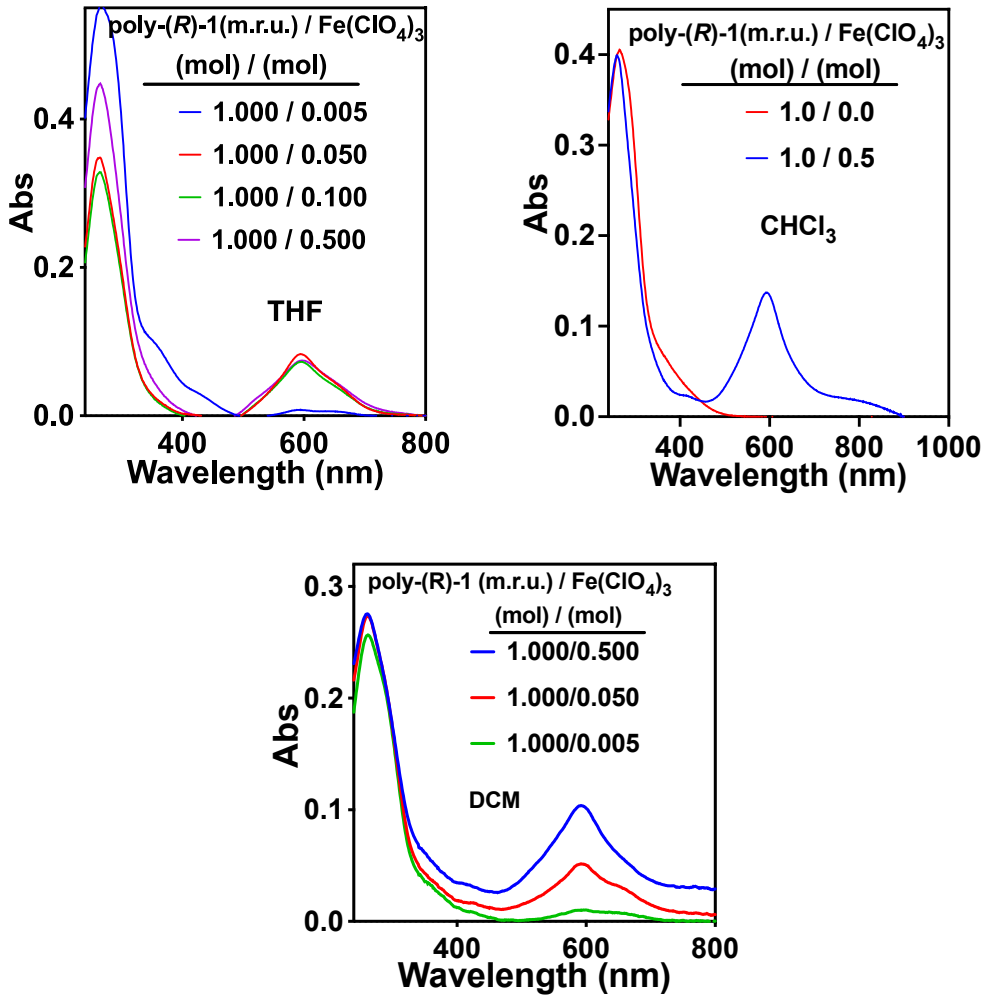

Figure S5. UV-Vis of poly-(*R*)-**1** (0.1 mg mL^{-1}) in THF, $CHCl_3$ and DCM in presence of $Fe(ClO_4)_3$ (10 mg mL^{-1}, THF).

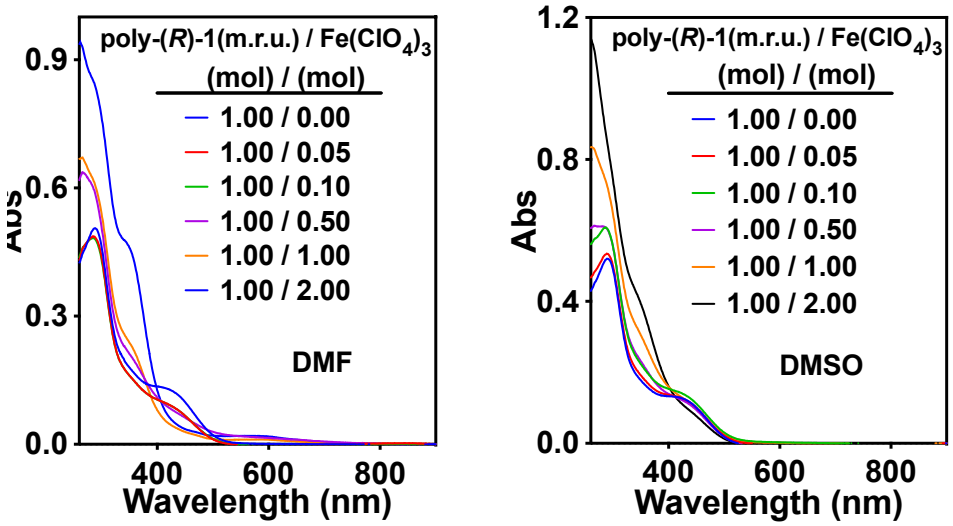

Figure S6. UV-Vis of poly-(*R*)-**1** (0.1 mg mL^{-1}) in DMF and DMSO in presence of $Fe(ClO_4)_3$ (10 mg mL^{-1}, THF).

6. FT-IR studies of poly-(*R*)-1 in presence of $Fe(ClO_4)_3$

A solution of $Fe(ClO_4)_3$ (0.5 equiv, 10.0 mg mL^{-1} in THF) was added to a solution of poly-(*R*)-**1** in THF (0.3 mg mL^{-1}) and then the FT-IR spectrum was registered. The experiments confirmed the coordination of Fe^{3+} ions to the carbonyl groups in poly-(*R*)-**1**.

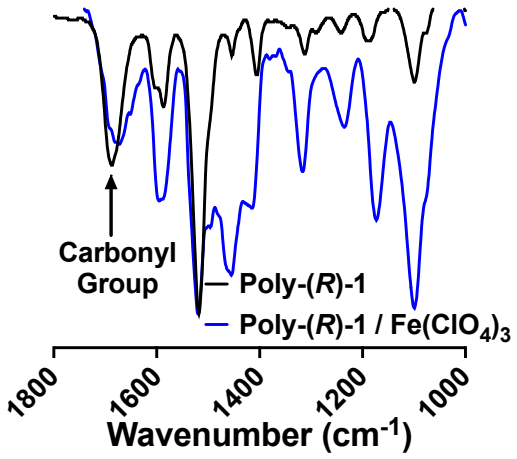

Figure S7. FT-IR spectra of poly-(*R*)-**1** and poly-(*R*)-**1**/$Fe(ClO_4)_3$.

7. UV-Vis and CD studies of poly-(*R*)-1 in presence of $FeCl_3$ in inert conditions.

UV-Vis and CD were performed for poly-(*R*)-**1** in THF in Argon using $FeCl_3$ which concentration 10.0 mg mL^{-1} THF.

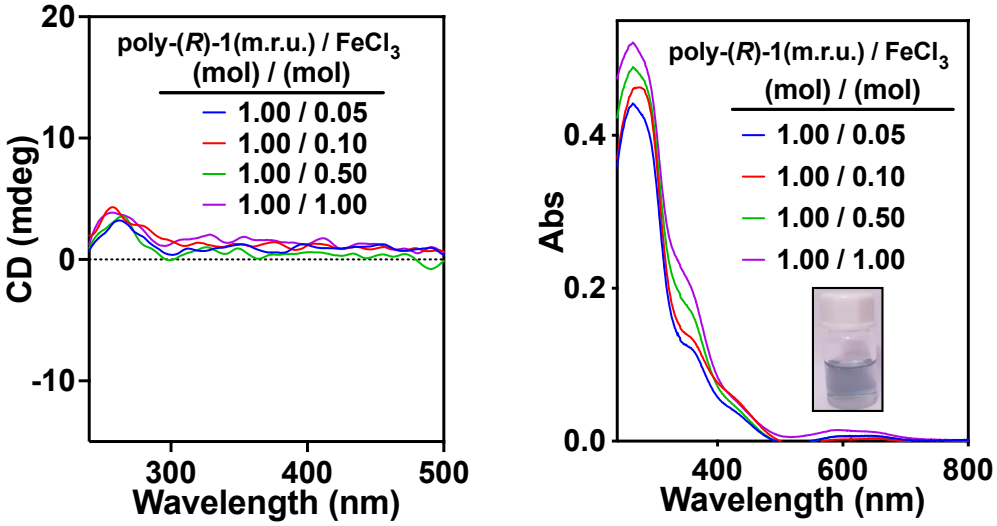

Figure S8. CD and UV-Vis of poly-(*R*)-**1** (0.1 mg mL^{-1} THF) in Argon in the presence of $FeCl_3$ (10 mg mL^{-1}, THF).

8. IR experiments of poly-(*R*)-1 in presence of $FeCl_3$ salt

solution of $FeCl_3$ (0.5 equiv, 10.0 mg mL^{-1} in THF) was added to a solution of poly-(*R*)-**1** in THF (0.3 mg mL^{-1}) and hen the FT-IR spectrum were registered.

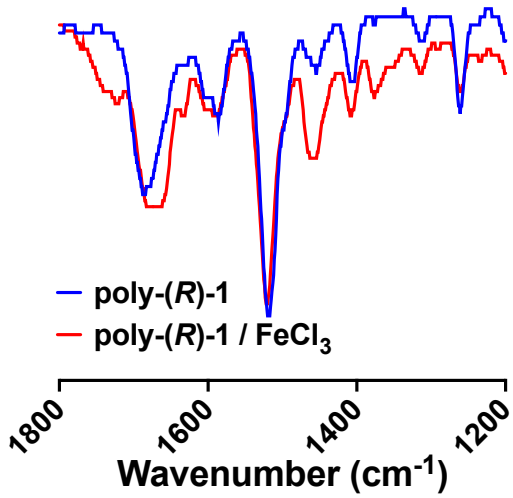

Figure S9. FT-IR spectra of poly-(*R*)-**1** and poly-(*R*)-**1**/$FeCl_3$.

9. UV-Vis studies of anilide-PPAs connection in presence of different oxidizing metal ions

UV-Vis were performed for poly-(*R*)-**1** (0.1 mg mL^{-1}) in THF using $Cu(ClO_4)_2$, $Fe(ClO_4)_3$, $Hg(ClO_4)_2$, and $AuCl_3$ which concentration was 1.0 mg mL^{-1} and 10.0 mg mL^{-1} in THF. Also $(NH_4)_2[Ce(NO_3)_6]$ was added with concentration 1.0 mg mL^{-1} and 10.0 mg mL^{-1} in MeOH.

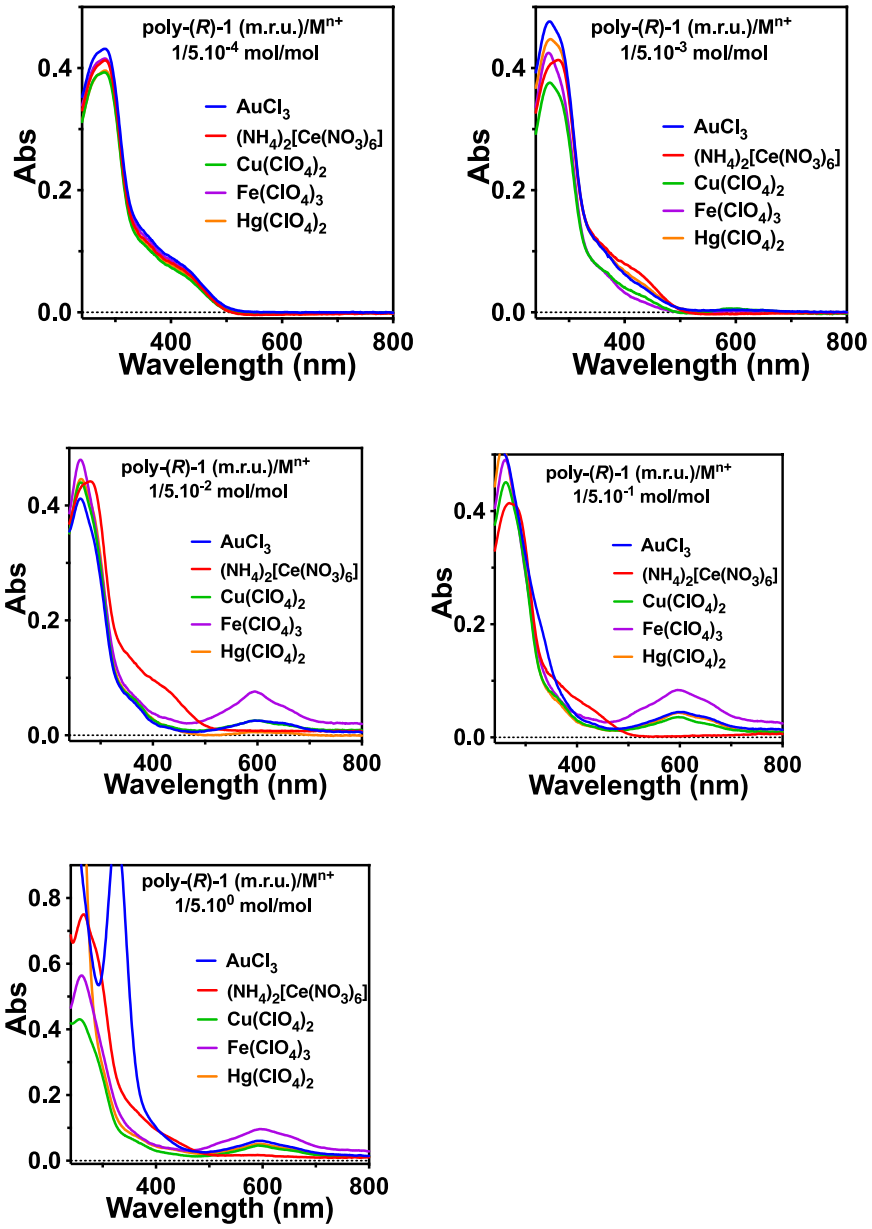

Figure S10. UV-Vis of poly-(*R*)-**1** (0.1 mg mL^{-1}) in THF in presence of different amounts of $Cu(ClO_4)_2$, $Fe(ClO_4)_3$, $Hg(ClO_4)_2$, and $AuCl_3$ (10 mg mL^{-1} and 1.0 mg mL^{-1} THF) or $(NH_4)_2[Ce(NO_3)_6]$ (10 mg mL^{-1} and 1 mg mL^{-1} MeOH).

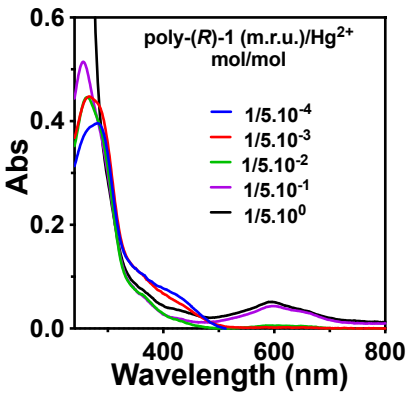
poly-(R)-1 (m.r.u.)/Hg2+
mol/mol
1/5.10-4
1/5.10-3
1/5.10-2
1/5.10-1
1/5.100
Abs
Wavelength (nm)

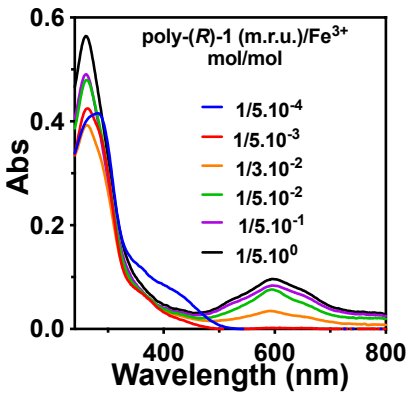
poly-(R)-1 (m.r.u.)/Fe3+
mol/mol
1/5.10-4
1/5.10-3
1/3.10-2
1/5.10-2
1/5.10-1
1/5.100
Abs
Wavelength (nm)

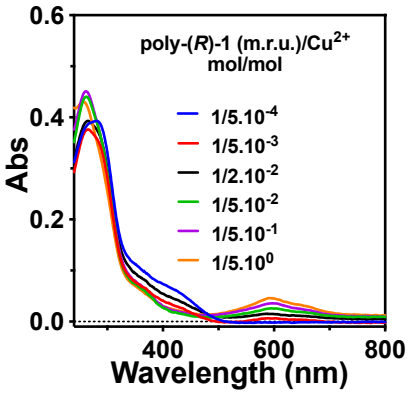
poly-(R)-1 (m.r.u.)/Cu2+
mol/mol
1/5.10-4
1/5.10-3
1/2.10-2
1/5.10-2
1/5.10-1
1/5.100
Abs
Wavelength (nm)

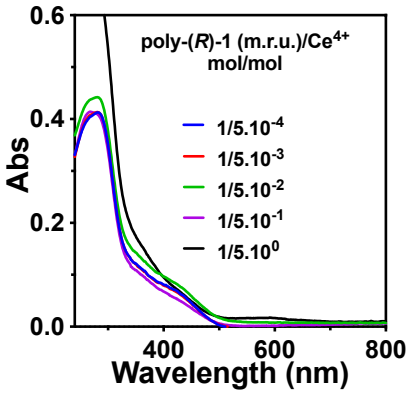
poly-(R)-1 (m.r.u.)/Ce4+
mol/mol
1/5.10-4
1/5.10-3
1/5.10-2
1/5.10-1
1/5.100
Abs
Wavelength (nm)

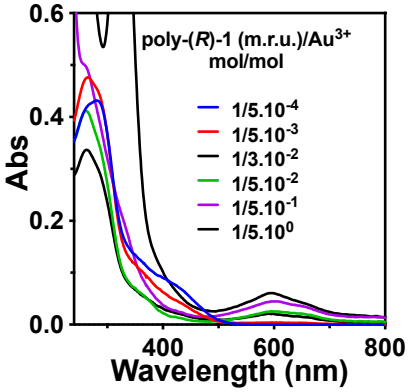
poly-(R)-1 (m.r.u.)/Au3+
mol/mol
1/5.10-4
1/5.10-3
1/3.10-2
1/5.10-2
1/5.10-1
1/5.100
Abs
Wavelength (nm)

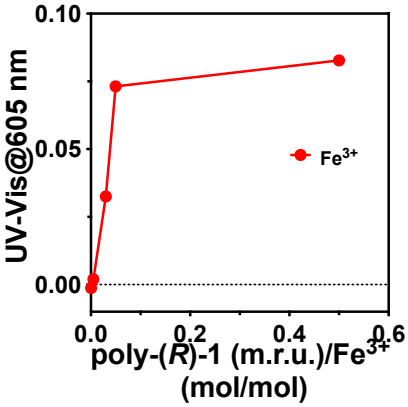
Fe3+
UV-Vis@605 nm
poly-(R)-1 (m.r.u.)/Fe3+
(mol/mol)

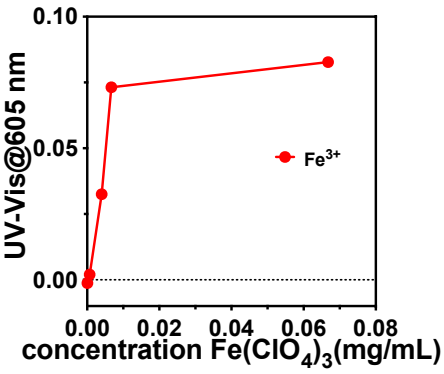
Fe3+
UV-Vis@605 nm
concentration Fe(ClO4)3(mg/mL)

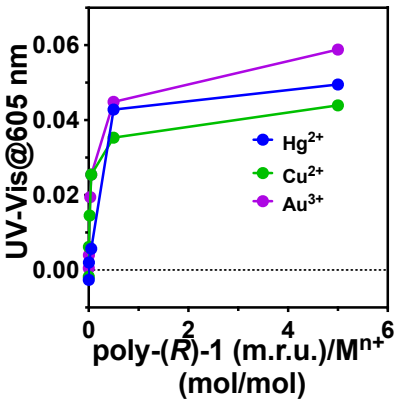
Hg2+
Cu2+
Au3+
UV-Vis@605 nm
poly-(R)-1 (m.r.u.)/Mn+
(mol/mol)

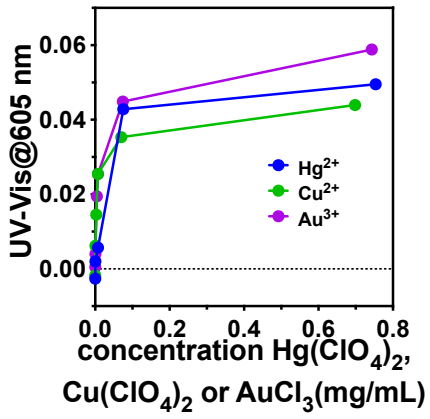

Figure S11. UV-Vis and response of the radical band at 605 nm of poly-(*R*)-**1** (0.1 mg mL^{-1}) in THF in presence of different equivalents of $Cu(ClO_4)_2$, $Fe(ClO_4)_3$, $Hg(ClO_4)_2$, and $AuCl_3$ (10 mg mL^{-1} and 1 mg mL^{-1} THF) or $(NH_4)_2[Ce(NO_3)_6]$ (10 mg mL^{-1} and 1.0 mg mL^{-1} MeOH).

10. UV-Vis studies of anilide-PPAs connection in presence of $Fe(ClO_4)_3$

CD studies and UV-Vis were performed with poly-(*R*)-**2** and poly-(*R*)-**3** (0.3 mg mL^{-1}, THF or $CHCl_3$) using $Fe(ClO_4)_3$ which concentration was 10.0 mg mL^{-1}.

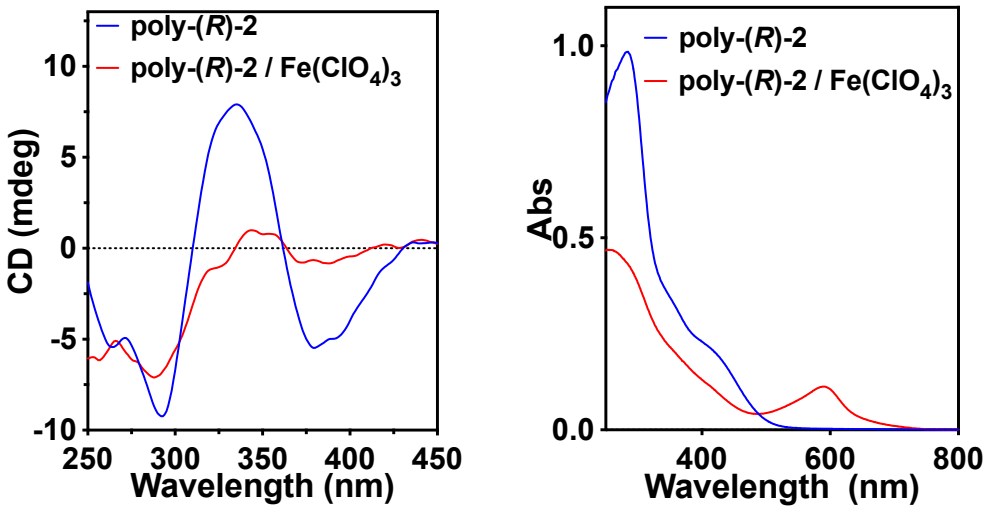

Figure S12. CD and UV-Vis experiments of poly-(*R*)-**2** (0.3 mg mL^{-1}, THF) in presence of 0.5 equiv of Fe^{3+} (10 mg mL^{-1}, THF).

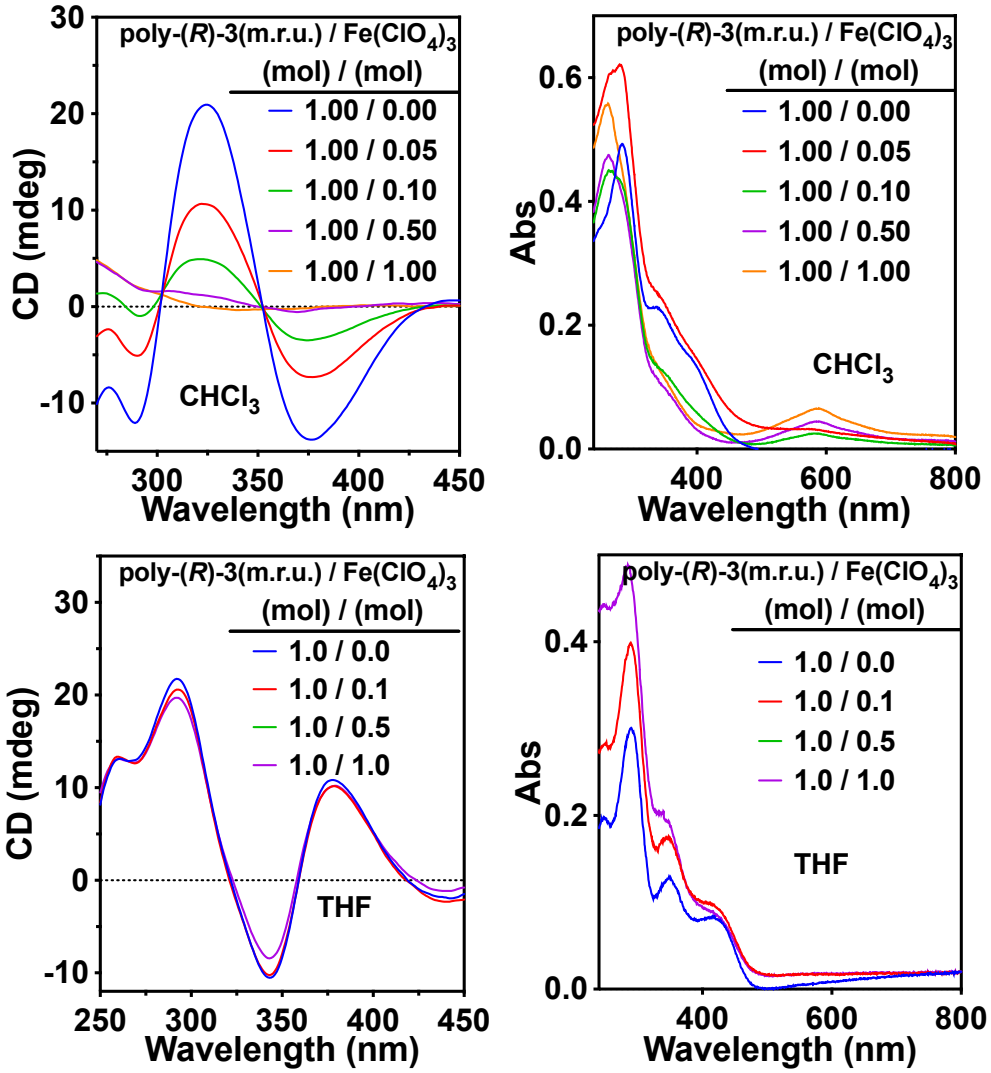

Figure S13. CD and UV-Vis experiments of poly-(*R*)-**3** (0.3 mg mL^{-1}, $CHCl_3$ and THF) in presence of $Fe(ClO_4)_3$ (10 mg mL^{-1}, THF).

11. CD and UV-Vis studies of benzamide-PPAs connection in presence of $Fe(ClO_4)_3$

CD studies and UV-Vis were performed with a poly-(*S*)-**4**, poly-(*S*)-**5** and poly-(*S*)-**6** (0.3 mg mL^{-1}, THF) using $Fe(ClO_4)_3$ which concentration was 10.0 mg mL^{-1}.

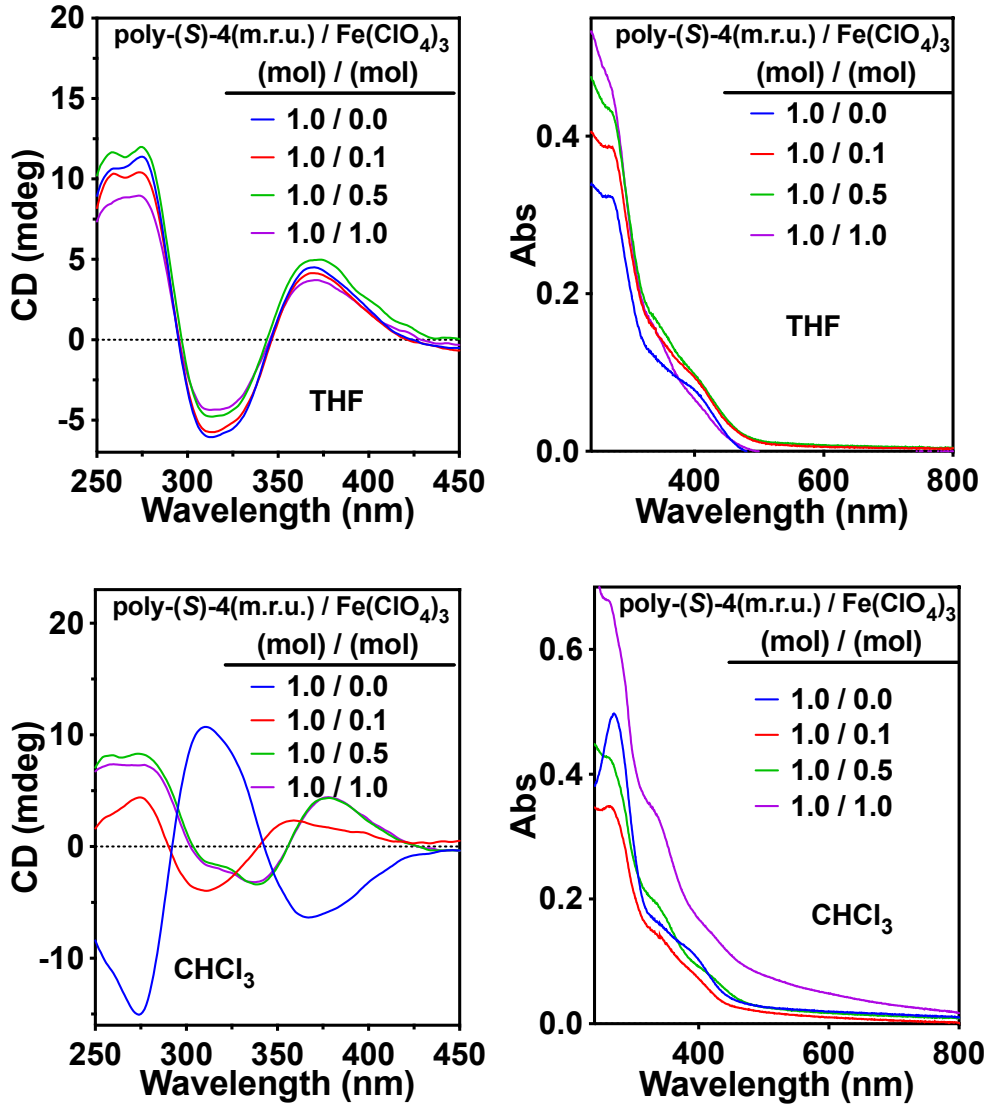

Figure S14. CD and UV-Vis experiments of poly-(*S*)-**4** (0.3 mg mL^{-1}, THF and $CHCl_3$) in presence of $Fe(ClO_4)_3$ (10 mg mL^{-1}, THF).

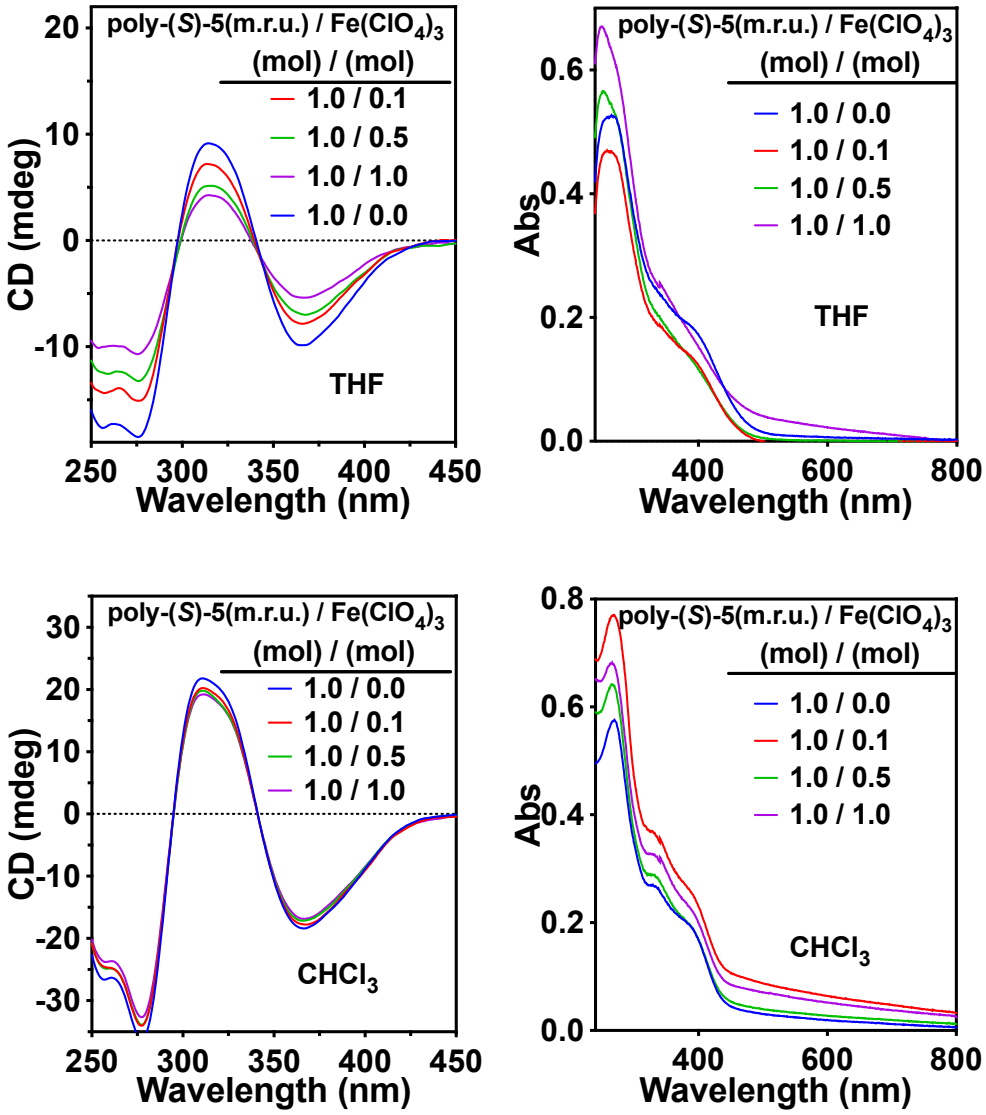

Figure S15. Cd and UV-Vis experiments of poly-(*S*)-**5** (0.3 mg mL^{-1}, THF and $CHCl_3$) in presence of $Fe(ClO_4)_3$ (10 mg mL^{-1}, THF).

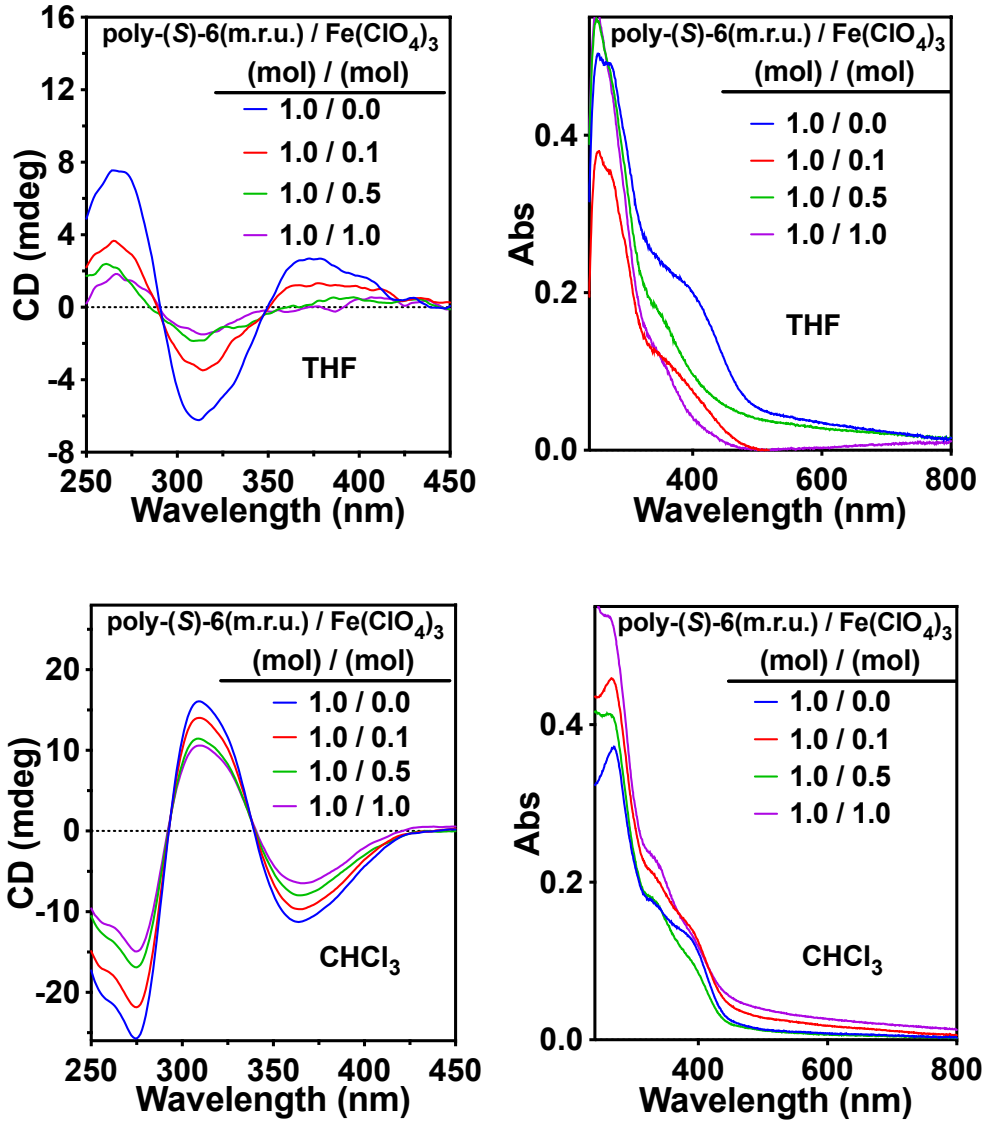

Figure S16. Cd and UV-Vis experiments of poly-(*S*)-**6** (0.3 mg mL^{-1}, THF and $CHCl_3$) in presence of $Fe(ClO_4)_3$ (10 mg mL^{-1}, THF).

12. CD and UV-Vis studies of benzamide-PPAs connection in presence of $Fe(ClO_4)_3$

CD studies and UV-Vis were performed with of poly-(*S*)-**4** (0.3 mg mL^{-1}, $CHCl_3$ and THF) using $Fe(ClO_4)_3$ which concentration was 10.0 mg mL^{-1} in THF.

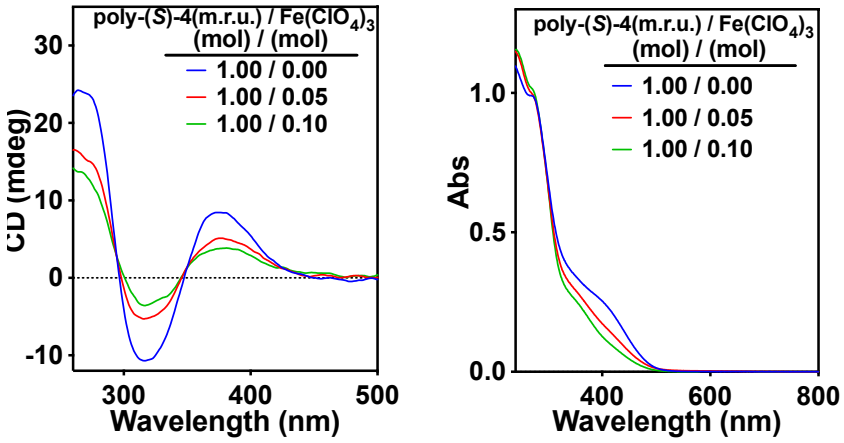

Figure S17. CD and UV-Vis studies of poly-(*S*)-**4** (0.3 mg mL^{-1}, THF) in presence of $Fe(ClO_4)_3$ (10 mg mL^{-1}, THF).

13. EPR studies of anilide and benzamide-PPAs connection

EPR experiments were carried out to study the presence of radicals in poly-(*R*)-**3**, poly-(*R*)-**5**, poly-(*S*)-**5**, poly-(*R*)-**7**, **M-1** and (3 mg mL^{-1}, THF) after addition of $Fe(ClO_4)_3$ (10 mg mL^{-1}, THF).

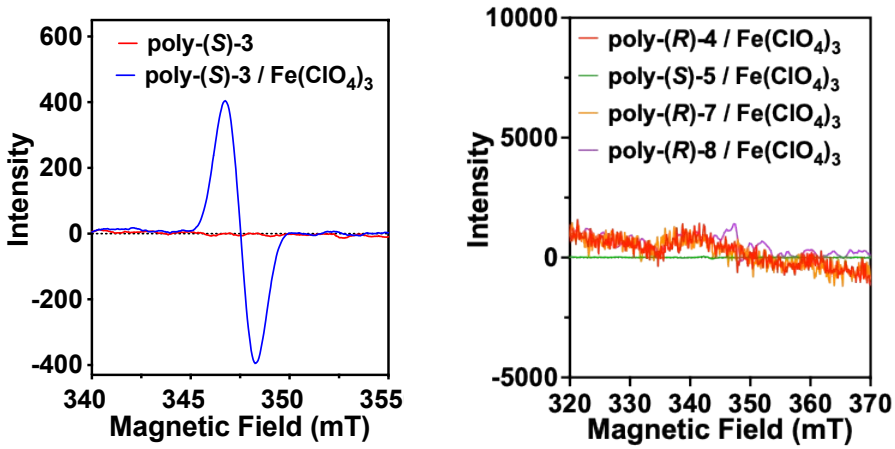

Figure S18. EPR experiments of **M-1**, poly-(*R*)-**3**, poly-(*R*)-**4**, poly-(*S*)-**5**, and poly-(*R*)-**7** (3.0 mg mL^{-1}, THF) in presence of $Fe(ClO_4)_3$ (0.01 equiv, 10.0 mg mL-1 in THF).

14. CD and UV-Vis studies of M-(*R*)-1 in presence of $Fe(ClO_4)_3$

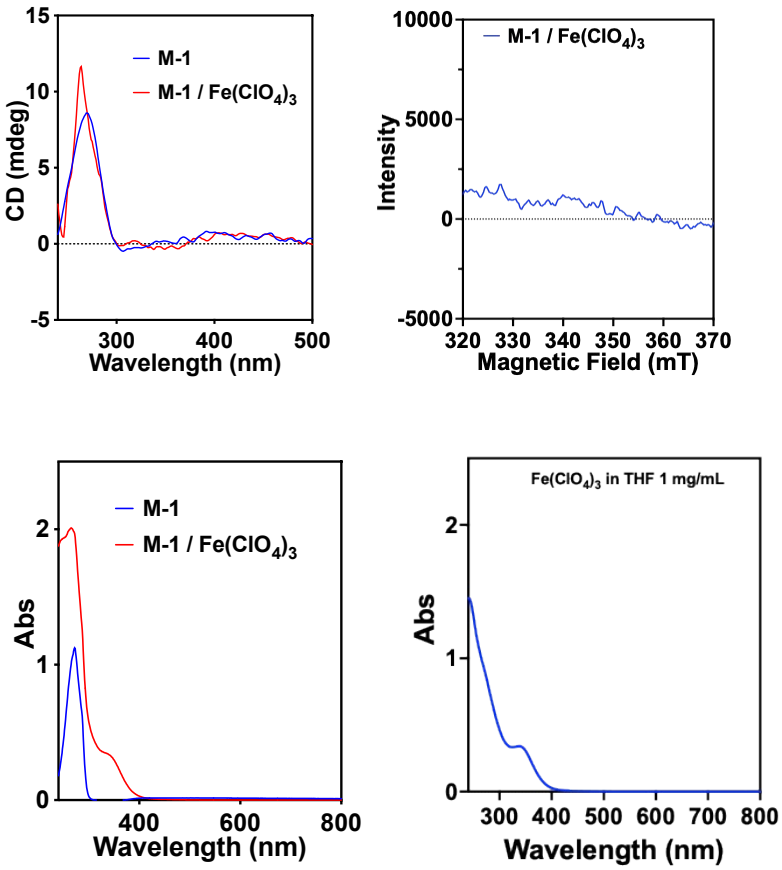

Figure S19. CD, UV-Vis studies of M-**1** (0.3 mg mL^{-1}, THF) in presence of $Fe(ClO_4)_3$ (1 mg mL^{-1}, THF). UV-Vis spectrum of $Fe(ClO_4)_3$ in THF. EPR studies of M-**1** (3.0 mg mL^{-1}, THF) in presence of $Fe(ClO_4)_3$ (0.01 equiv, 10.0 mg mL^{-1}, THF)

15. CD and UV-Vis studies of poly-(*R*)-7 in presence of $Fe(ClO_4)_3$

CD and UV-Vis studies of poly-(*R*)-**7** (0.1 mg mL^{-1}, THF) were carried out in in presence of $Fe(ClO_4)_3$ (10 mg mL^{-1}, THF).

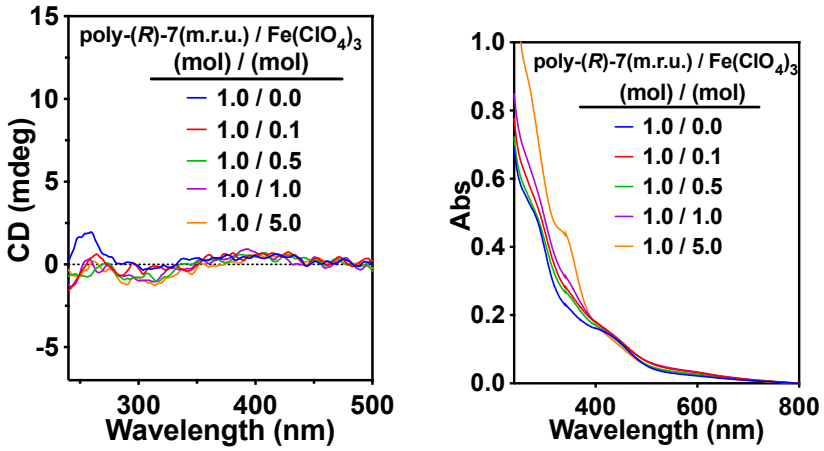

Figure S20. CD and UV-Vis studies of poly-(*R*)-**7** (0.1 mg mL^{-1}, THF) in presence of different amounts of $Fe(ClO_4)_3$ (10 mg mL^{-1}, THF).

16. IR experiments of poly-(*R*)-7 in presence of $Fe(ClO_4)_3$ salt

A solution of $Fe(ClO_4)_3$ (0.5 equiv, 10.0 mg mL^{-1} in THF) was added to a solution of poly-(*R*)-**7** in THF (0.3 mg mL^{-1}) and hen the FT-IR spectra were registered. The experiments confirmed the coordination of Fe^{2+} and Fe^{3+} to the carbonyl groups in poly-(*R*)-**7**.

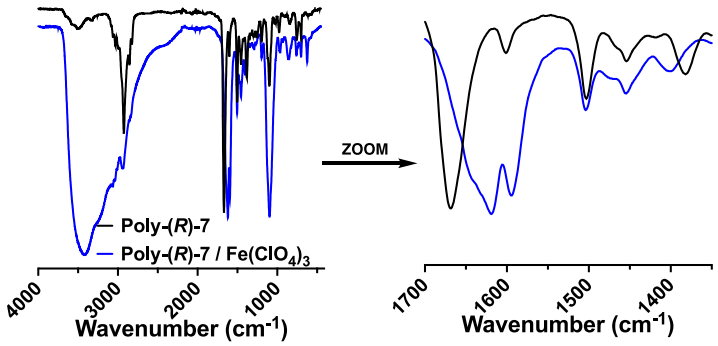

Figure S21. FT-IR spectra of poly-(*R*)-**7** and poly-(*R*)-**7**/$Fe(ClO_4)_3$.

17. UV-Vis studies of poly-(*R*)-1 in presence of different M^{2+}

UV-Vis were performed for poly-(*R*)-**1** (0.1 mg mL^{-1}, THF) using $M(ClO_4)_2$ which concentration was 10.0 mg mL^{-1}.

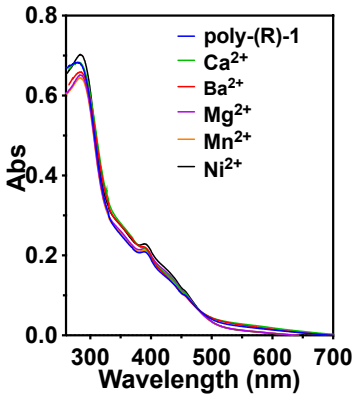

Figure S22. UV-Vis experiments of poly-(*R*)-**1** (0.1 mg mL^{-1}, THF) in presence of 0.1 equiv of $M(ClO_4)_2$ (10 mg mL^{-1}, THF).

18. UV-Vis studies of poly-(*R*)-1 and poly-(*R*)-3 titration with $Fe(ClO_4)_3$

UV-Vis were performed for poly-(*R*)-**1** and poly-(*R*)-**3**(0.1 mg mL^{-1}, $CHCl_3$) using $Fe(ClO_4)_3$ which concentration was 1.0 mg mL^{-1} in THF.

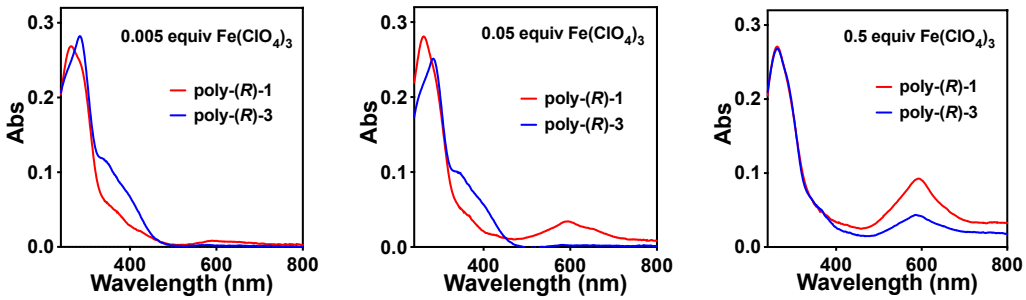

Figure S23. UV-Vis experiments of poly-(*R*)-**1** and poly-(*R*)-**3**(0.1 mg mL^{-1}, $CHCl_3$) in presence of $Fe(ClO_4)_3$ (1.0 mg mL^{-1}, THF).

19. UV-Vis studies of poly-(*R*)- in presence of $Fe(ClO_4)_3$

UV-Vis were performed for poly-(*R*)-**1** (0.1 mg mL^{-1}) using 0.01 equiv of $Fe(ClO_4)_3$ (1.0 mg mL^{-1}, THF) in mixtures of $CHCl_3$/THF (v/v).

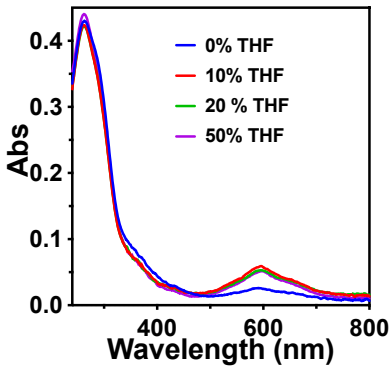

Figure S24. UV-Vis experiments of poly-(*R*)-**1** (0.1 mg mL^{-1}, THF/$CHCl_3$) in presence of 0.01 equiv of $Fe(ClO_4)_3$ (1.0 mg mL^{-1}, THF).

20. Density functional theory-based computations

Gaussian-16 (G16RevC.01) [S4] was used to compute n=8 oligomers of poly-(*R*)-**1** with *trans*-configuration of double bonds, and the same calculation were carried out for a n=9 oligomer of poly-(*R*)-**1** with a *cis*- configuration of double bonds. The restricted closed-shell and unrestricted open-shell B3LYP [S5] functionals together with the basis set 6-31G(d) [S6] were used to perform the DFT [S7] calculations. Geometry optimizations and frequency calculations of the oligomers were performed with charge +1 and doublet multiplicity in the unrestricted open-shell calculations while charge 0 and singlet multiplicity was used the restricted closed-shell calculations without imaginary frequencies and spin contamination. TD-DFT calculations were performed using the cam-b3lyp functional with the 6-31G(d) basis set. UV-vis spectra were simulated with 150 excitations, unrestricted calculations have 0,33 ev of peak half-width at half height and the restricted one for the non-radical structure has 0,20 ev.

For the EPR/ESR calculations, orca 4.1.2 [S8] in the UKS B3LYP with the EPR-II basis set [S9] were performed for the g tensor with the absence of the A-tensor (hyperfine coupling). Prop files were processed in easyspin 5.2.35 [S10]. These approximations were calculated with the garlic function, which computes isotropic and fast-motional EPR spectra of radicals in solution. The simulation was performed at 298 K, Lorentzian linewidths of 1mT and the experimental field sweep frequencies of 9,790 GHz.

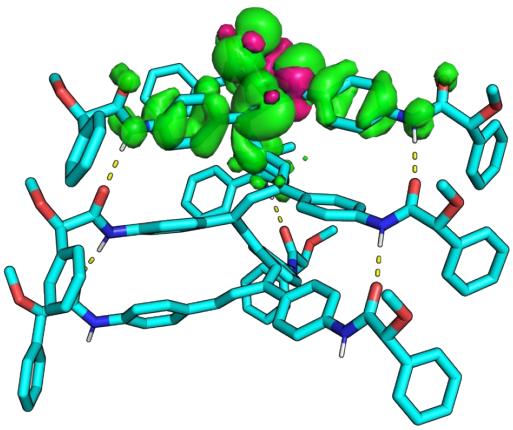

Figure S25. Calculated Spin Density of the cation radical *cis-cisoidal* structure without delocalization of the radical.

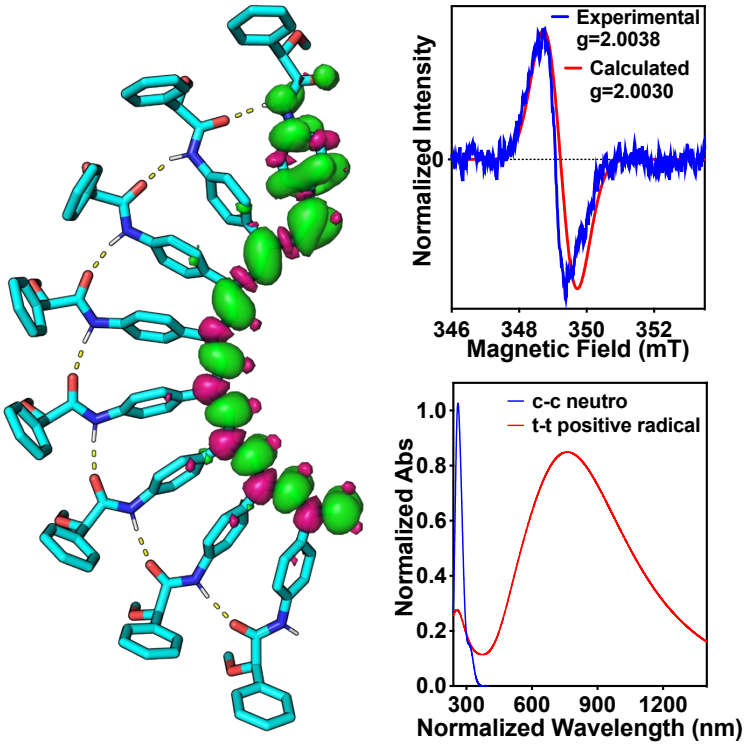

Figure S26. Calculated Spin density, EPR and UV-Vis (compared with neutral *cis-cisoidal* structure) of the cation radical *trans-transoidal* structure.

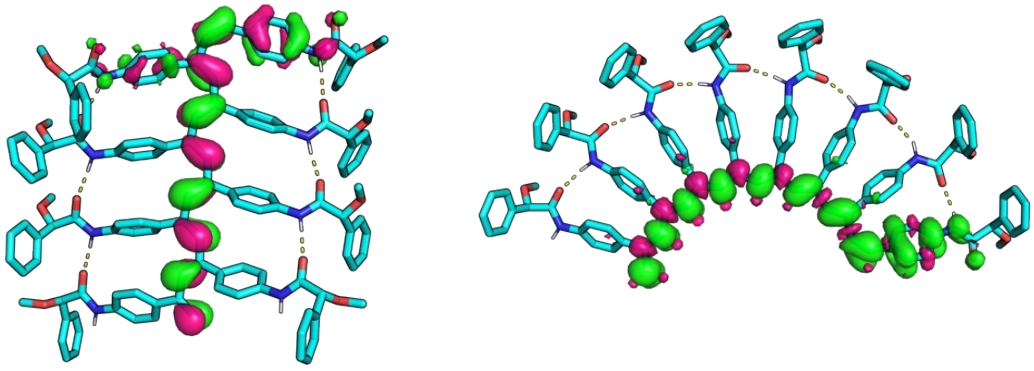

Figure S27. Calculated HOMO(/SOMO) of the radical cation *trans-cisoidal* and *trans-transoidal* configuration of the double bonds.

21. Calculation of the limits of detection

The limit of detection (LOD) for the radical formation in poly-(*R*)-**1** (100 mg/L, THF) was calculated in presence of various oxidants: $Cu(ClO_4)_2$, $Fe(ClO_4)_3$, $Hg(ClO_4)_2$, and $AuCl_3$. First, standard deviations of the residuals ($SD_{residuals}$) and the intercept ($SD_{intercept}$) using Equations (1) and (2) were calculated:

$$SD_{residuals} = \sqrt{\frac{\sum_{i=1}^{n}(y_i - \hat{y}_i)^2}{n-2}} \quad (1)$$

$$SD_{intercept} = SD_{residuals} * \sqrt{\frac{\sum_{i=1}^{n} x_i^{\,2}}{n * \sum_{i=1}^{n}(x_i - \bar{x})^2}} \quad (2)$$

Where y_i and $\hat{y}_i$ are the absorbance in UV-Vis at 609 nm corresponding to radical formation in the PPA and predicted absorbance, x_i represents the concentration of oxidants in (mg/L), $\bar{x}$ is the mean of x_i , and n is the number of data points. The resulting values for $SD_{residuals}$ and $SD_{intercept}$, along with the slopes (m) obtained from the linear regression, are summarized in Table 1.

For the linear regression, only the data from the initial concentrations (Figure S11) were used, where the UV-Vis absorbance of the radical polymer at 605 nm showed a linear response corresponding to radical formation. At higher oxidant concentrations, the polymer became saturated, and the absorbance no longer increased, deviating from linearity. The resulting fits, limited to the linear region, are displayed in Figure S28.

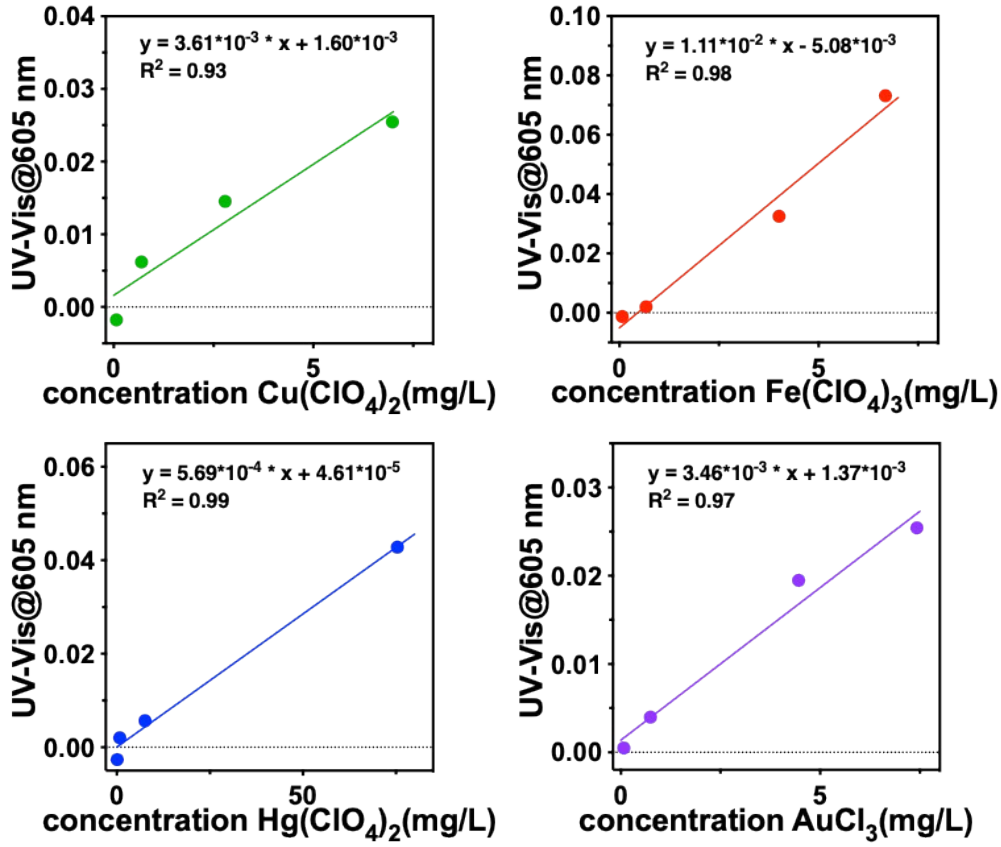

Figure S28. UV-Vis absorbance at 605 nm of the polymer (0.1 mg/mL in THF) at varying concentrations of $Cu(ClO_4)_2$, $Fe(ClO_4)_3$, $Hg(ClO_4)_2$, and $AuCl_3$, with linear fits for the initial range, including the equation and R^2. Saturation occurs at higher concentrations.

Table S1. Regression Parameters and Standard Deviations

Oxidant	$SD_{residuals}$ (Abs)	$SD_{intercept}$, (Abs)	m (Abs L/mg)
$Cu(ClO_4)_2$	$3.71x10^{-3}$	$2.59x10^{-3}$	$3.61x10^{-3}$
$Fe(ClO_4)_3$	$6.07x10^{-3}$	$4.44x10^{-3}$	$1.11x10^{-2}$
$Hg(ClO_4)_2$	$2.42x10^{-3}$	$1.45x10^{-3}$	$5.69x10^{-4}$
$AuCl_3$	$2.36x10^{-3}$	$1.72x10^{-3}$	$3.46x10^{-3}$

Using these values, the LOD was calculated according to Eq. (3):

$$LOD = \frac{SD}{m} \tag{3}$$

Where SD is $SD_{intercept}$, and m is the slope. The results, expressed in both ppm (m/v) (mg/L) and ppm (m/m) (mg/kg) using the density of THF (0.888kg/L), are presented in Table 2.

Table S2. Calculated Limits of Detection (LOD)

Oxidant	$LOD_{intercept}$ (m/v) (mg/L)	$LOD_{intercept}$ (m/m) (mg/kg)
$Cu(ClO_4)_2$	2.37	2.67
$Fe(ClO_4)_3$	1.32	1.49
$Hg(ClO_4)_2$	8.41	9.47
$AuCl_3$	1.65	1.85

22. UV-Vis studies of poly-(*R*)-1 in presence of H_2O_2

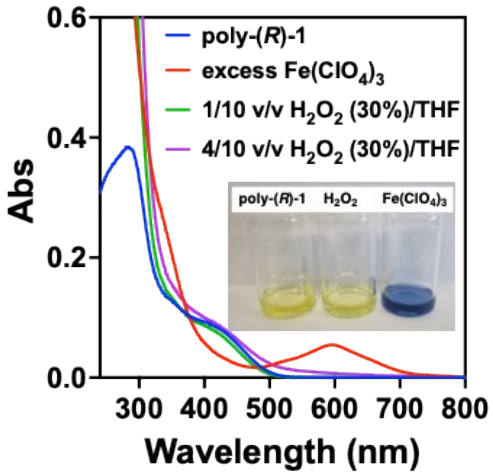

Figure S29. UV-Vis absorbance of poly-(*R*)-**1** in 1 mL THF (0.1 mg/mL), in the presence of excess of $Fe(ClO_4)_3$, and excess of H_2O_2 (30%).

22. Time Dependent UV-Vis Studies

Time dependent (TD) UV-Vis studies were carried out for a THF solution of poly-(*R*)-**1** (0.1 mg/mL) after addition of an oxidizing metal salt. Thus, variations in the UV-Vis band at 600 nm corresponding to the organic radical were plotted versus time after injection of 0.5 and 0.05 equiv. of $Fe(ClO_4)_3$ (Figure 30a), $Cu(ClO_4)_2$ (Figure 30b), $Hg(ClO_4)_2$ (Figure 30c) and $Au(ClO_4)_3$ (Figure 30d). In all cases the presence of a new UV band at 600 nm is observed once the metal salt is added. However, from these studies we observed that poly-(*R*)-**1** shows the best response towards Fe^{3+}, where the UV band is one order of magnitude higher than when the other metal ions are used. In case of Cu^{2+}, Hg^{2+} and Au^{3+} the UV band at 600 nm corresponding to the organic radical increases with time but does not reach the value obtained with Fe^{3+}.

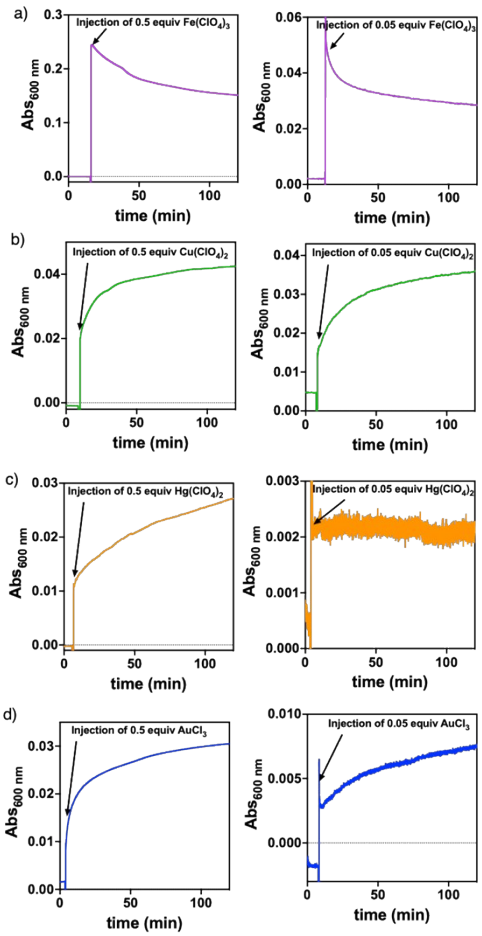

Figure S30. TD-UV-Vis studies of a THF solution of poly-(*R*)-**1** (0.1 mg/mL) in the presence of 0.5 and 0.05 equiv of (a) $Fe(ClO_4)_3$, (b) $Cu(ClO_4)_2$, (c) $Hg(ClO_4)_2$ and (d) $Au(ClO_4)_3$.

22. References

S1. R. Rodríguez, E. Quiñoá, R. Riguera, F. Freire, *J. Am. Chem. Soc.* **2016**, *138*, 9620–9628.

S2. S. Leiras, F. Freire, J. M. Seco, E. Quiñoá, R. Riguera, *Chem. Sci.* **2013**, *4*, 2735-2743.

S3. S. Arias, M. Núñez-Martínez, E. Quiñoá, R. Riguera, F. Freire*, Polym. Chem.* **2017**, *8*, 3740–3745.

S4. Gaussian 16, Revision C.01, M. J. Frisch, G. W. Trucks, H. B. Schlegel, G. E. Scuseria, M. A. Robb, J. R. Cheeseman, G. Scalmani, V. Barone, G. A. Petersson, H. Nakatsuji, X. Li, M. Caricato, A. V. Marenich, J. Bloino, B. G. Janesko, R. Gomperts, B. Mennucci, H. P. Hratchian, J. V. Ortiz, A. F. Izmaylov, J. L. Sonnenberg, D. Williams-Young, F. Ding, F. Lipparini, F. Egidi, J. Goings, B. Peng, A. Petrone, T. Henderson, D. Ranasinghe, V. G. Zakrzewski, J. Gao, N. Rega, G. Zheng, W. Liang, M. Hada, M. Ehara, K. Toyota, R. Fukuda, J. Hasegawa, M. Ishida, T. Nakajima, Y. Honda, O. Kitao, H. Nakai, T. Vreven, K. Throssell, J. A. Montgomery, Jr., J. E. Peralta, F. Ogliaro, M. J. Bearpark, J. J. Heyd, E. N. Brothers, K. N. Kudin, V. N. Staroverov, T. A. Keith, R. Kobayashi, J. Normand, K. Raghavachari, A. P. Rendell, J. C. Burant, S. S. Iyengar, J. Tomasi, M. Cossi, J. M. Millam, M. Klene, C. Adamo, R. Cammi, J. W. Ochterski, R. L. Martin, K. Morokuma, O. Farkas, J. B. Foresman, and D. J. Fox, Gaussian, Inc., Wallingford CT, **2016**.

S5. A. D. Becke, *The Journal of Chemical Physics* **1993**, *98*, 5648–5652.

S6. V. A. Rassolov, M. A. Ratner, J. A. Pople, P. C. Redfern, L. A. Curtiss, *J Comput Chem* **2001**, *22*, 976–984.

S7. P. Hohenberg, W. Kohn, *Phys. Rev.* **1964**, *136,* 864-871.

S8. F. Neese, *WIREs Comput Mol Sci* **2011**, *2*, 73–78.

S9. V. BARONE, *Recent Advances in Density Functional Methods* **1995**, 287–334.

S10. S. Stoll, A. Schweiger*, Journal of Magnetic Resonance* **2006**, *178*, 42–55.